

RSC Advances



This is an *Accepted Manuscript*, which has been through the Royal Society of Chemistry peer review process and has been accepted for publication.

Accepted Manuscripts are published online shortly after acceptance, before technical editing, formatting and proof reading. Using this free service, authors can make their results available to the community, in citable form, before we publish the edited article. This *Accepted Manuscript* will be replaced by the edited, formatted and paginated article as soon as this is available.

You can find more information about *Accepted Manuscripts* in the [Information for Authors](#).

Please note that technical editing may introduce minor changes to the text and/or graphics, which may alter content. The journal's standard [Terms & Conditions](#) and the [Ethical guidelines](#) still apply. In no event shall the Royal Society of Chemistry be held responsible for any errors or omissions in this *Accepted Manuscript* or any consequences arising from the use of any information it contains.

Synthesis and Characterization of Poly(γ -glutamic acid)-based Alumina Nanoparticles with Their Protein Adsorption Efficiency and Cytotoxicity Towards Human Prostate Cancer Cell

Running Head: Protein adsorption and cytotoxicity of functionalized nanoalumina

Yesudoss Christu Rajan¹, Baskaran Stephen Inbaraj¹ and Bing Huei Chen^{1,2,*}

¹ Department of Food Science

² Graduate Institute of Medicine

Fu Jen University, Taipei 242, Taiwan

*** Corresponding author**

Prof.B.H.Chen
Department of Food Science
Fu Jen University
Taipei 242, Taiwan
Tel.: +886-2-29053626
Fax: +886-2-29051215
Email: 002622@mail.fju.edu.tw

Abstract

Metal oxide nanoparticles, especially alumina nanoparticles (AN) have drawn considerable attention in biotechnological and biomedical applications. Interaction of nanoparticles with protein plays a crucial role in several medical applications. Also, nanoparticles may exert toxic effects on cancer cells that can be beneficial for application in cancer therapy. The objectives of this study were to synthesize and characterize poly(γ -glutamic acid) (γ -PGA)-functionalized alumina nanoparticles (γ -PAN) for evaluation of protein adsorption ability using bovine serum albumin (BSA) and lysozyme (LSZ) as well as cytotoxicity towards human prostate cancer cell PC-3. Characterization of both AN and γ -PAN revealed a spinel lattice structure belonging to γ -Al₂O₃ with the mean particle size as determined by TEM being 5.4 nm for AN and 6.7 nm for γ -PAN. Zeta potential at different pH changed from positive to negative upon coating γ -PGA onto AN with a shift in point-of-zero-charge from 9.1 to 3.2 mV. Positively-charged AN at pH 7 could preferentially adsorb BSA compared to LSZ, while an opposite trend was observed for negatively-charged γ -PAN. The Langmuir adsorption capacity for AN and γ -PAN was 224.5 and 36.1 mg/g for BSA, respectively, and 16.2 and 110.1 mg/g for LSZ. Both AN and γ -PAN could lower cell viability of PC-3 cells in a dose-dependent manner with the latter more efficient than the former. The ROS production also increased with dose, which may lead to cytotoxicity towards PC-3 cells through oxidative stress and mitochondrial dysfunction. Thus, the γ -PGA functionalized alumina nanoparticles may be used as a promising material for future biomedical applications.

Keywords: Alumina nanoparticles, poly(γ -glutamic acid), protein adsorption, cytotoxicity, prostate cancer cell.

1. Introduction

Nanotechnology has become an area of significant interest due to the diverse range of its application in fields such as medicine, industry, agriculture and public health in the past two decades.^{1,2} Metal oxide nanoparticles, especially alumina nanoparticles (AN), are a future promising material in biotechnological and biomedical applications as they are hydrolytically stable, bioinert and can be readily surface-functionalized.³ For instance, AN have been applied in several areas including catalysis, structural ceramics, functionalization of textiles, wastewater treatment and protein separation and purification.⁴⁻⁷ Also, AN find wide biological applications in biosensors, biofiltration, drug delivery, and antigen delivery for immunization purposes.^{8,9} Compared to other metal oxide nanoparticles, the synthesis of AN is simple, inexpensive, and the raw materials used are cost effective and readily available.^{10,11} Among several synthesis methods available, both precipitation and sol-gel methods are the most commonly used.¹¹ In addition, several reaction parameters including pH, temperature, time and precursor concentration play a vital role to obtain AN of desired shape and size.¹² In this study, a precipitation-digestion method was adopted to synthesize γ -alumina nanoparticle of uniform size by controlling both temperature and pH.

Interaction of nanoparticles with carbohydrates, proteins, nucleic acids, lipids or other metabolites has recently drawn considerable attention, particularly the nanoparticle-protein interaction in biological and medical applications. Upon administration during diagnostics or drug delivery, a significant number of proteins can be adsorbed onto the nanoparticle surface resulting in formation of nanoparticle-protein complex commonly referred as the nanoparticle-protein corona.¹³ Therefore, it is necessary to learn how proteins interact with nanoparticle both in vitro and in vivo. Several studies have been performed dealing with proteins adsorption on bare AN and surface modified AN.¹⁴⁻¹⁶ Song *et al.*¹⁷ studied adsorption of bovine serum albumin (BSA) on various metal oxide nanoparticles and

reported that BSA adsorption depended on several parameters including surface area, hydrophilicity of nanoparticle surface and electrostatic attraction between BSA and particle surface. In a similar study Meder *et al.*¹⁵ modified AN with different functional groups for comparison of adsorption efficiency of BSA, lysozyme (LSZ) and trypsin (TRY), and the result showed that BSA was preferentially adsorbed on positively charged surface of AN and AN-NH₂, while LSZ and TRY adsorbed on negatively charged AN-COOH, AN-SO₃ and AN-PO₃H₂. Moreover, several parameters including zeta potential, surface characteristics, concentration, and acidity or basicity of functional groups, all of which were shown to influence adsorption of glutathione on surface-tailored AN to a certain degree.¹⁸ In addition, some functionalized nano porous AN have been widely used in the efficient separation of biomolecules such as proteins and DNA.^{4,19} Thus, it is pivotal to study the protein adsorption by synthesized nanoparticles so that the nanoparticle-protein interactions can be elucidated.

The toxicity of metal and metal oxide nanoparticles towards environment, animal and human remains a major health concern owing to the increased use of nanoparticles and accumulation in the environment. Thus, the terminology 'nanotoxicology' was introduced to study the toxic effects and interactions of the nanoparticles with biological systems. When metal oxide nanoparticles interact with cells, reactive oxygen species (ROS) are generated resulting in pro-inflammatory reactions and enhancement of oxidative stress via intracellular signalling pathways.²⁰ Nanoparticles can readily enter the cell membrane and accumulate in the cytoplasm, leading to disruption of metabolism, cell dysfunction and even cell death.²¹ Lin *et al.*⁵ demonstrated a dose- and time-dependent decrease in cell viability after incubation of bronchoalveolar carcinoma-derived cells with 13 or 22 nm AN. In a similar study the AN were shown to exhibit significant toxicity towards L929 cells through multiple mechanisms such as mitochondrial dysfunction, oxidative stress and cell death.²² Chen *et al.*²³ further reported that AN could alter mitochondrial potential, induce cellular oxidative stress (ROS),

and decrease the expression of tight junction proteins to a greater extent than bulk or carbon nanoparticles. However, in a recent study, Yang *et al.*²⁴ have demonstrated a low toxicity in mice orally-fed with AN with no significant absorption or imbalance in essential elements. In the present study we examined the cellular toxicity of AN and γ -PGA coated AN (γ -PAN) toward prostate cancer cells PC-3 by MTT assay and monitored generation of intracellular ROS at the same time by using the fluorescent probe CM-H₂DCFDA.

It has been well established that surface modification of metal oxide nanoparticles with various functional groups can not only prevent aggregation, but also improve the chemical stability, biocompatibility, therapeutic efficiency, versatility, selectivity and adsorption properties.^{10,25} More importantly, the retention of any organic compound on unmodified AN is not feasible owing to its weak interaction with the hydrophilic nature of AN surface. Thus, some physical or chemical modifications of AN surface with certain functional groups containing electron donor atoms is necessary.¹⁰ For instance, Bertazzo *et al.*²⁶ have shown that ethanedioic acid could alter the bioactivity of AN through interaction with nanoparticle surface. Likewise, the adsorption capacity of AN for organic compounds was shown to improve greatly through deposition of humic acid onto AN surface.²⁷ In a later study Meder *et al.*¹⁶ further demonstrated that through modification of the AN surface with different density of sulfonate groups, protein adsorption could be controlled.

In the present study, a non-toxic and biodegradable biopolymer poly(γ -glutamic acid) (γ -PGA) was used as a basis for functionalization with AN surface. The γ -PGA has been widely used as a biomaterial in the fields of medicine, pharmaceuticals, cosmetics, food industry and environmental science.²⁸⁻³⁰ Currently, γ -PGA can be synthesized in different ionic forms and varying molecular weights by fermentation using *Bacillus* species. More recently, Stevanović *et al.*³¹ used γ -PGA as a stabilizer to synthesize metal nanoparticles and found that they were biocompatible and did not induce any toxicity toward Caco-2 epithelial cells.

Thus, in addition to favoring the interaction of nanoparticles with living cells, γ -PGA can also act as a particle stabilizer in several biomedical applications.³² In several previous studies we evaluated the metal detoxifying effect of both pure γ -PGA and γ -PGA coated magnetic nanoparticles as well as the antibacterial activity.^{28,29,33} However, to the best of our knowledge, no data are currently available on nanoparticle toxicity and protein adsorption capacity with respect to γ -PGA-based AN and toxicity towards prostate cancer cell. The objectives of this study were to synthesize and characterize both bare AN and γ -PAN for evaluation of protein adsorption efficiency and cytotoxicity towards human prostate cancer cells PC-3.

2. Experimental

2.1. Materials

The chemical reagents aluminium sulfate ($\text{Al}_2(\text{SO}_4)_3$) (99.9%) and ammonia (28%) used for synthesis of AN were obtained from Sigma-Aldrich (St. Louis, MO) and J.T. Baker (Phillipsburg, USA), respectively. The soluble form of γ -PGA (NaPGA) used for functionalization of AN was procured from Vedan Enterprise Corp. (Taichung, Taiwan). Alkali metal salts potassium bromide (95%) and sodium chloride (>99%) used for FTIR and zeta potential studies, respectively, were purchased from Nacalai Tesque (Kyoto, Japan) and J.T. Baker. The pH was adjusted during synthesis by using hydrochloric acid (35%) and sodium hydroxide (95%) from Nacalai Tesque. Ethanol (95%) used for washing the precipitated AN was from Taiwan Tobacco and Wine Bureau (Tainan, Taiwan). For protein adsorption experiments, model proteins bovine serum albumin ($\geq 90\%$) and lysozyme ($\geq 90\%$) were obtained from Sigma, while Coomassie® brilliant blue G-250 dye reagent ($\geq 80\%$) for protein assay was from Bradford Laboratories (Bossier city, LA, USA). A fluorescence dye 5-(and 6-)-chloromethyl-2,7-dichlorodihydro fluorescein diacetate ($\geq 90\%$) added for measuring intracellular ROS formation was from Molecular Probes (Eugene, OR). For

cytotoxicity study, prostate cancer cell line PC-3 was obtained from American Type Culture Collection Center (ATCC, VA, USA). Cell-culture medium Dulbecco's Modified Eagle Medium (DMEM), 2.5% trypsin-EDTA and penicillin–streptomycin were all procured from Invitrogen (CA, USA). Fetal bovine serum (FBS) was from HyClone (UT, USA), while phosphate buffered saline, dimethyl sulfoxide (DMSO) and 3-[4,5-dimethylthiazol-2-yl]-2,5 diphenyl tetrazolium bromide (MTT) reagent (98%) were all from Sigma-Aldrich. The deionized water was obtained from a Milli-Q system from Millipore Co. (Bedford, MA, USA).

The instruments employed for synthesis of alumina nanoparticles and γ -PGA coated alumina nanoparticles include a Suntex 701 pH meter (Suntext Instruments Co., Ltd, Taipei, Taiwan) coupled with a 9611-10D model glass electrode from Horiba Instruments Inc. (CA, USA),²⁴ magnetic stirrer (SP46925, Thermolyne-Cimarec-2, IA, USA), ultrasonicator (Delta DC-400H, Tech-Lab Scientific, Malaysia), muffle furnace (S.J. High Technologies Co., Taipei, Taiwan), hot-air oven (Shen Long Instruments, Taipei, Taiwan), centrifuge (5810R, Eppendorf, Hamburg, Germany) and freeze dryer (FD24, Chin-Ming Co., Taipei, Taiwan). For protein adsorption experiments, a B601D reciprocating water bath shaker from Firstek Scientific Co. (Tau Yen, Taiwan)²⁸ and a DU 640 spectrophotometer from Beckman Instruments (CA, USA)³⁴ were used. Likewise, several instruments used for cytotoxicity study include laminar flow hood (4BC-24, Jau-Hsin, Taipei, Taiwan), carbon dioxide incubator (SCA-165DS, Astec, Fukuoka, Japan), ELISA reader (Versa Max, Molecular Devices, CA, USA),^{28,35} while a SpectraMax Gemini microplate spectrofluorometer from Molecular Devices (CA, USA) was used for ROS determination.³⁵

2.2. Synthesis of γ -alumina particles

A precipitation–digestion method based on Potdar *et al.*³⁶ was modified and used for synthesis of AN. The synthesis involved precipitation of aluminum sulfate by addition of a

base. Briefly, 0.1 M aluminum sulfate solution was prepared in a 1 L beaker by dissolving 17.10 g in 500 mL of deionized water and stirred well for complete dissolution of aluminium salt. Then, ammonia solution (28%) was added drop-wise to the solution until the pH reached around 8.0 for precipitation of aluminum hydroxide. The stirring was continued at 70°C for 3 h and pH was maintained between 7 and 8 to produce nanoparticles of uniform size. Finally, the precipitate was centrifuged, followed by washing three times with deionized water and one time with alcohol, drying at 50°C for 24 h in a hot-air oven. The air-dried powder was then calcined in a programmable furnace at 800°C for 1 h to produce AN.

2.3. Functionalization of γ -alumina particles

The as-synthesized AN were functionalized based on a method described by Meder *et al.*³ with slight modification. Initially, a clear suspension of AN was prepared by mixing 1.5 g γ -alumina with 10 mL of deionized water (1.5 mM) and sonicating for 30 min. Next, 0.18 mM γ -PGA solution was prepared by dissolving 0.18 g in 10 mL deionized water and then added to AN suspension. The resulting suspension was stirred at room temperature for 60 min and then subjected to heating at 60°C for 90 min, after which the particles obtained were separated by centrifuging and washed three times with 20 mL of deionized water to remove residual free γ -PGA. After separation, the nanoparticles were freeze-dried under vacuum for 48 h at -20°C.

2.4. Characterization of γ -alumina and γ -PGA coated γ -alumina nanoparticles

The Fourier transform infrared spectra of boehmite (AlOOH), pure γ -PGA, AN, and γ -PAN were recorded and compared by using a Horiba FTIR spectrophotometer (FT 730, Kyoto, Japan). Each sample was homogenized with KBr crystals, pelletized at a pressure of 150 kg/cm² and mounted on the sample holder for recording spectra in the frequency range of 4000–400 cm⁻¹. A total of 32 interferograms at a resolution of 2 cm⁻¹ was measured for each sample.^{11,28,36} The X-ray diffraction pattern of AN and γ -PAN was recorded on a Multiflex

model Rigaku diffractometer (Tokyo, Japan) in the 2θ range of $20\text{--}70^\circ$ using $\text{Cu-K}\alpha$ radiation ($\lambda = 1.540556$) at 40 kV and 40 mA.^{28,34,35} Also, the mean diameter of nanoparticles was determined by substituting full-width half-maximum of a XRD peak in the Scherrer equation.³⁷ To determine coating percentage of γ -PGA on AN, thermogravimetric analysis of nanoparticles was carried out by heating 5–10 mg of each sample from $25\text{--}900^\circ\text{C}$ at a rate of $10^\circ\text{C}/\text{min}$ in a versa Therm HS model Cahn thermogravimetric analyzer (Thermo Fischer Scientific, USA).^{28,34} The mean particle size and morphology of both nanoparticles were determined by capturing images in a JEOL transmission field emission electron microscope (TEM, JEM 2100F; JEOL, Ltd, Tokyo, Japan) at 120 kV. Sample preparation was carried out by spreading a drop of diluted aqueous suspension of each nanoparticle sample on a 150 mesh carbon-coated copper grid (Ted Pella Inc, Redding, CA) and vacuum-dried for 24 h.^{28,34,35} Scanning electron microscopic (SEM) images were also recorded by dispersing a few milligrams of each nanoparticle sample in water and casting $1\ \mu\text{L}$ of dispersed sample on a silicon wafer.²⁹ Then, the samples were dried overnight followed by coating with platinum using Auto Fine Coater (JEO, JFC-1600, Japan) at 10 mA for 90 s and capturing images using a JEOL JSM-6700F SEM instrument (Japan) at 10 kV. In addition, the energy dispersive X-ray spectroscopy (EDX, X-max, Oxford Instruments, Oxfordshire, U.K.) was recorded in the mapping mode to confirm γ -PGA coating on AN.²⁹ Additionally, the zeta potential was determined by dispersing 0.1 g/L of each nanoparticle sample in 0.001 M sodium chloride solutions adjusted to different pH values (2, 3, 4, 5, 6, 7, 8, 9, 10 and 11).²⁸ Then, each sample was measured for zeta potential by using a Malvern Zetasizer Nano ZS machine (Malvern Instruments Ltd, Worcestershire, UK).

2.5. Protein adsorption experiments

An adsorption method based on Song *et al.*¹⁷ and Sasidharan *et al.*³⁸ was modified and used for determination of protein adsorption capacity of pure γ -PGA, AN and γ -PAN. Briefly,

10 mL each from 8 different concentrations of BSA or LSZ (50, 100, 500, 1000, 2000, 3000, 4000 and 5000 mg/L) were collected and each solution was adjusted to pH 7.0. Then, 100 mg of AN or γ -PAN was added to the solution, followed by shaking at 50 rpm in a 37°C water bath shaker for 2 h, centrifuging at 4000 rpm for 10 min, and collecting supernatant for determination of protein by using a Bradford reagent assay with detection at 595 nm. Prior to protein adsorption experiment, a calibration curve was prepared for BSA and LSZ standards with a concentration range from 200–900 mg/L and 100–1500 mg/L, respectively. The protein adsorption capacity at equilibrium was determined based on the mass balance equation,^{28,29} $q_e = (C_i - C_e) / (V/W)$, where C_i is initial protein concentration, V (L) is the volume of protein solution, W (g) weight of AN or γ -PAN, C_e (mg/L) is protein concentration at equilibrium and q_e is adsorption capacity at equilibrium. The equilibrium data were fitted with a classical Langmuir isotherm by using a GNU PLOT program (Copyright Thomas Williams and Collin Kelley, version 4.0 for Windows) through a nonlinear regression method based on Marquardt-Levenberg algorithm.^{28,29} The non-linear form of the Langmuir equation can be represented as shown below:^{28,29}

$$q_e = \frac{K_L C_e}{1 + K_e C_e}$$

where, K_L (L/g) is a product of q_{\max} (mg/g) and K_e (L/mg), representing maximum adsorption capacity and equilibrium constant or adsorption energy, respectively.

2.6. Cytotoxicity against prostate cancer cell (PC-3)

2.6.1. Cell culture

Human prostate cancer cell line (PC-3) was cultured in Dulbecco's Modified Eagle Media (DMEM) supplemented with 10% heat-inactivated fetal bovine serum (FBS), 100 μ g/ml streptomycin, 100 UI/ml penicillin and grown at 37°C in a humidified incubator containing 5% CO₂. After 80% confluence was attained, cells were detached by mixing with

0.25% trypsin-EDTA solution for 5 min and aliquots of the separated cells were subcultured as 1:5 splits.

2.6.2. MTT assay

The MTT assay is a simple and non-radioactive assay commonly employed to determine cell viability and proliferation of cells. It involves determination of mitochondrial activity spectrophotometrically by measuring a colored formazan derivative formed through metabolic reduction of MTT reagent by the mitochondrial dehydrogenase enzyme present in living cells. Based on a method reported by Inbaraj *et al.*,³³ cytotoxicity of AN and γ -PAN was determined by seeding 4000 exponentially growing cells into 100 μ L of medium in a 96 well plate and incubated for 24 h at 37°C in a humidified incubator containing 5% CO₂ to allow attachment of cells. After 24 h, medium was replaced by fresh medium containing different concentrations (0.01, 0.02, 0.03, 0.06, 0.13, 0.25, 0.50 and 1.00 mg/mL) of AN and γ -PAN separately and incubated for 48 h. To evaluate cell survival, 200 μ L of 0.5 mg/mL MTT reagent was added to each well and incubated for 4 h for formation of formazan crystals. Medium containing MTT was then gently replaced by 100 μ L of DMSO to solubilize formazan crystals. The plates were further incubated for 24 h for complete dissolution of the formazan crystals and the absorbance was measured at 550 nm on an ELISA reader. To check if nanoparticles interfere with the optical density (OD) values, the OD measurements were taken again after transferring the supernatant of each well to a new 96-well plate. The plate reader was calibrated to zero absorbance using the culture medium without cells and the relative cell viability (%) as compared to control wells containing medium without nanoparticles was calculated using a formula, $[\text{Abs}]_{\text{nanoparticle}} / [\text{Abs}]_{\text{control}} \times 100$, where $[\text{Abs}]_{\text{nanoparticle}}$ and $[\text{Abs}]_{\text{control}}$ represent absorbance value obtained for nanoparticle and control samples, respectively.³³

2.7. Intracellular reactive oxygen species determination

The generation of intracellular ROS was determined based on a method reported by Babu *et al.*,³⁵ which involves measurement of oxidative conversion of the non-fluorescent material, CM-H₂DCFDA, to a highly fluorescent compound dichlorofluorescein (DCF). Initially, cells were seeded on a 96 well plate at a density of 2×10^3 cells per well in 100 μ l of medium. After 24 h of incubation at 37°C and 5% CO₂, cells were exposed separately to various concentrations (0.01, 0.02, 0.03, 0.06, 0.13, 0.25, 0.50 and 1.00 mg/mL) of AN and γ -PAN for 48 h, washed three times with phosphate-buffered saline (PBS) and incubated with 10 μ M CM-H₂DCFDA for 1 h at 37°C. Cells were then washed and the DCF was measured immediately using a microplate reading spectrofluorometer at an excitation and emission wavelength of 490 and 545 nm, respectively, with cells without nanoparticles being used as control. To monitor the change in cell morphology, phase contrast images were captured using inverted microscope for control PC-3 cells, control PC-3 cells treated with ROS detecting reagent CM-H₂DCFDA only, cells treated with different doses (0.01, 0.03, 0.13, 0.25, 0.50 and 1.00 mg/mL) of AN or γ -PAN alone and along with ROS detecting reagent CM-H₂DCFDA.

2.8. Statistical analysis

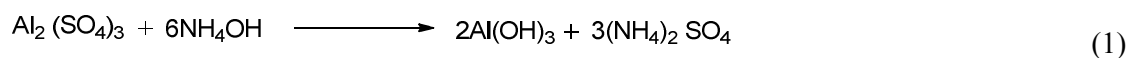
All experiments were done in triplicate and the data were subjected to ANOVA analysis and Duncan's multiple range test for significance ($P < 0.05$) in mean comparison by Statistical Analysis System.³⁹

3. Results and discussion

3.1. Synthesis of γ -alumina nanoparticles

As mentioned before, alumina nanoparticles have become a promising material in both fields of biomedicine and biotechnology as they can be used for protein separation and purification, fabrication of biomedical devices and drug delivery.^{3,5,27} Many chemical methods including sol-gel, emulsion, precipitation and hydrothermal have been reported for

synthesis of AN.¹⁰ Of the various methods, precipitation is a simple one and widely employed for production of nano-sized porous alumina particles.¹¹ Therefore, in this study, a precipitation-digestion method was adopted for preparation of AN nanoparticles, which involved the following three steps: (1) A dropwise addition of ammonia into aluminium sulfate solution resulting in formation of a transparent gel-like aluminium hydroxide precipitate between pH 7 and 8 at 70°C as shown in reaction 1.



(2) The white-gel like precipitate was then digested at 70°C for 3 h with simultaneous stirring and maintaining of pH between 7 and 8 in order to convert $\text{Al}(\text{OH})_3$ into crystalline boehmite precursor AlOOH as shown in reaction 2.



(3) After filtering, washing and drying, boehmite AlOOH was calcined at 800°C for 1 h to obtain AN as shown in reaction 3.



To further functionalize and improve colloidal stability, the AN nanoparticles were coated with carboxyl-rich γ -PGA as described in the previous section.

3.2. Characterization of γ -alumina and γ -PGA coated γ -alumina nanoparticles

3.2.1. X-ray diffraction spectrometry

The XRD patterns for both AN and γ -PAN showed 6 diffraction peaks corresponding to the Bragg reflections (1 1 1) at 22.4°, (2 2 0) at 34.5°, (3 1 1) at 37.9°, (4 0 0) at 45.6°, (5 1 1) at 62.2° and (4 4 0) at 66.7°, indicating that γ - Al_2O_3 with a spinel lattice structure was synthesized (Figure 1).³⁶ Moreover, the broadening of peaks caused by small crystallite sizes revealed that γ - Al_2O_3 particles are both nano-sized and crystalline in nature.³⁶ Based on the full-width of a diffraction peak at half-maximum intensity (β), the crystallite size (d) size of

nanoparticles was determined by using the Scherrer equation,³⁹ $d = k\lambda / \beta \cos\theta$, where k is a constant (~ 0.9), λ is the wavelength of $\text{CuK}\alpha$ radiation (1.5406 Å) and θ is the Bragg angle. The crystallite size was calculated to be 3.8 and 4.5 nm for AN and γ -PAN, respectively. A similar particle size of 3.8 nm and 4.7 nm was reported by Naskar⁴⁰ for AN obtained after calcination at 550°C and 800°C, respectively. However, Rahmanpour *et al.*⁴¹ have shown a relatively lower particle size of 1–2 nm for AN synthesized by calcination at 550°C, while Potdar *et al.*³⁶ reported a particle size range of 3.5–4.5 nm for AN obtained upon calcination at the same temperature.

3.2.2. Transmission electron microscopy

Figures 2A and 2B depict the TEM images of AN and γ -PAN recorded at 120 kV. The morphology of both AN and γ -PAN is roughly spherical in shape with the former being relatively more agglomerated compared to the latter. Obviously, the alumina nanoparticles have an inherent tendency to agglomerate due to strong vander Waal's forces which becomes predominant during calcination at a high temperature (800–1200°C), as pointed out by Naskar.⁴⁰ In addition, the gelatinous form of alumina nanoparticles may facilitate their agglomeration.¹¹ However, a significant deagglomeration of AN could be achieved by functionalizing with appropriate coating materials like γ -PGA. The particle size distribution histogram obtained directly from the TEM image revealed the mean particle size to be 5.4 nm for γ -AN and 6.7 nm for γ -PAN, which was close to that (3.8 and 4.5 nm) determined by the Scherrer equation using XRD data.

3.2.3. Scanning electron microscopy

Scanning electron microscopic images were recorded to observe changes after coating of AN with γ -PGA (Figures 3A1 and 3B1). Besides, the EDX spectrum in the mapping mode was captured to compare the proportion of aluminium, carbon and oxygen (Figures A2-A4 and B2-B4). Apparently the surface of AN seems to be rough, while γ -PAN appears to be

smooth, probably caused by fine coating of γ -PGA onto AN surface. The observed tendency of as-synthesized alumina nanoparticles to agglomerate was also perceived in several SEM micrographs reported in different studies,^{11,36,42} which may be attributed to the reasons as mentioned above. Comparatively, the EDX images revealed approximately the same proportion of aluminium for both AN and γ -PAN, however, the proportion of carbon and oxygen rose upon coating of AN with γ -PGA (Figure 3A2-A4 and 3B2-B4). Obviously, γ -PGA being a coating material should incorporate more carbon and oxygen atoms onto the surface of AN, as γ -PGA is composed of numerous glutamic acid units connected by γ -amide linkage. This phenomenon corroborates with that reported in a recent study where a relatively high weight percentage of carbon (63.65%) and oxygen (29.53%) was shown in the EDX analysis of aluminium-adsorbed γ -PGA.²⁹

3.2.4. Fourier transform infrared spectrometry

The FTIR spectrum of boehmite and AN depicted a broad band at 3425 and 3472 cm^{-1} , respectively, along with an intense band at 1641 and 1645 cm^{-1} , both of which are typical of stretching and bending vibrations due to absorbed water (Figures 4A and 4B). In addition, the spectra for boehmite showed peaks at 615.2 and 485.4 cm^{-1} , which are characteristics of stretching and bending vibrations of AlO_6 , respectively, while a peak at 750.6 cm^{-1} is assigned to torsional vibration of OH group.^{11,36} Also, an intense peak at 1073.2 cm^{-1} and a shoulder at 1165.4 cm^{-1} for boehmite are associated with Al-O-Al symmetric and asymmetric bending modes of vibration, respectively (Figure 4A). Potdar *et al.*³⁶ showed analogues IR bands around 3447 and 1640 cm^{-1} for both boehmite and AN, while significant peaks at 1163, 1073, 750, 617 and 481 cm^{-1} was shown to occur for AN. After calcination of boehmite precursor, a very broad band (480–900 cm^{-1}) with two distinct peak areas appeared for AN in the frequency range 480–750 cm^{-1} and 750–900 cm^{-1} , which corresponded to Al-O vibrations in γ - Al_2O_3 with aluminium ions occupying the tetrahedral (γ - AlO_4) and octahedral (γ - AlO_6)

coordination sites (Figure 4B).^{11,36} On the other hand, the spectrum for pure γ -PGA revealed three representative peaks at 1625, 1565 and 1403 cm^{-1} , with the latter two peaks are indicative of asymmetric COO^- stretch and overlap peak of N-H/C-N deformation, respectively, while the symmetric stretching vibration of COO^- group represented the former peak (Figure 4C).^{28,33,34} After coating of AN with γ -PGA, peaks representing both bare AN and pure γ -PGA appeared in the spectrum of γ -PAN, confirming that γ -PGA coating did occur on AN surface (Figure 4D). Moreover, a rise in peak broadening around 3200–3600 cm^{-1} for pure γ -PGA and γ -PAN should be due to the deliquescent nature of water-soluble sodium form of γ -PGA. The difference in wavenumber between the intense bands at 1641 and 1645 cm^{-1} for boehmite and alumina nanoparticles (AN), respectively, seems to be negligible and may not be a peak shift. Moreover, it is quite possible as AN was formed after subjecting boehmite to calcination at 800°C. On the other hand, the peak-shift to lower wavenumber for pure γ -PGA (1625.8 cm^{-1}) and γ -PGA coated AN (1637.7 cm^{-1}) should be due to the overlap of peaks in Figure 4A and 4B with the more broader peaks corresponding to numerous carboxylic acid and amide groups in γ -PGA (Figure 4C) and γ -PGA coated AN (Figure 4D).

3.2.5. Thermogravimetry

The thermogravimetric analysis curves illustrated an initial loss of about 8% at temperature $<280^\circ\text{C}$ for both AN and γ -PAN, which are mainly caused by removal of absorbed water, volatile impurities and complete dehydration of precipitate (Figure 5). A similar trend in the temperature range of 230–260°C was reported for AN by Ghanta *et al.*,⁴³ who attributed the weight loss to the volatilization of organic residue attached on the AN surface. However, at $>300^\circ\text{C}$, no significant weight loss occurred for AN, while a rapid weight loss of about 12% observed only for γ -PAN, which should be attributed to evaporation followed by decomposition of γ -PGA coating on γ -PAN. Previous studies on the application

of γ -PGA as coating material for functionalizing iron oxide nanoparticles have reported a 7–8% weight loss for sodium salt of γ -PGA^{28,33} and 12% for calcium salt of γ -PGA.⁴⁴

3.2.6. Zeta potential measurements

Figure 6 shows the change in zeta potential of AN and γ -PAN as affected by different pH. With the exception of pH 10 and 11, the zeta potential of AN at most pH values (2-9) were positive, indicating the presence of positive charge on AN surface. On the contrary, a reversed trend was shown for γ -PAN with the surface charge being negative at pH 4-11 and positive at pH 2 and 3. Also, a decrease in zeta potential occurred for γ -PAN at all pH values (pH 1-11) when compared to AN. For instance, upon coating of AN with γ -PGA, the zeta potential at pH 7 decreased from +19.4 to -40.7 mV, which should be caused by dissociation of ionisable carboxylic acid groups in γ -PGA. A similar phenomenon was observed by Ghosh *et al.*,²⁷ reporting a drop in zeta potential from +35 mV to -33.5 mV at pH 8 upon coating of AN with humic acid. Consequently, in our study, the cross-over point from positive to negative zeta potential signified a decline in pH of zero point charge (pH_{zpc}) from 9.1 to 3.2 after coating of AN with γ -PGA (Figure 6), which was similar to that reported for bare AN (9.3) and methylsuccinic acid-functionalized AN (3.2) by Meder *et al.*¹⁵ Generally, the nanoparticle suspensions with zeta potential higher than +25 mV or lower than -25 mV are considered to be colloidally stable.¹⁰ In other words, according to classical DLVO theory, the aggregation of nanoparticles does not occur at pH value far from pH_{zpc} .⁴⁵ For AN with pH_{zpc} at 7.9, Ghosh *et al.*²⁷ pointed out by atomic force microscopy that AN dispersion did not show any size variation at pH 3 and 11, but tended to aggregate at pH 7. In our study, with the exception of pH 3 and 4, the zeta potential was $>+30$ mV for pH 2 and <-30 mV for the pH range from 5-11 for γ -PAN (Figure 6), suggesting that a greater colloidal stability could be attained at most environmental and biological pH values after coating of AN with γ -PGA.

3.3. Protein adsorption capacity

The formation of protein layer with tailored composition on nanoparticle surface is critical for biotechnological and biomedical applications such as carrier for enzyme, immunoassay, cell targeting and as biosensor.¹⁵⁻¹⁷ More specifically, the composition of protein layer modulate the nanoparticle's toxicity, performance, biocompatibility and selectivity in areas such as imaging and drug delivery as well as protein purification and separation.⁴⁶ Also, the preferential adsorption of proteins onto nanoparticle surface depends not only on the surface chemistry but also the protein properties. Thus, two model proteins BSA and LSZ with different structural properties were chosen for evaluating their adsorption on AN and γ -PAN. Batch-mode adsorption experiments conducted by taking a range of BSA or LSZ concentration (500–5000 mg/L) and shaking with 10 g/L of AN or γ -PAN separately at pH 7 and 37°C revealed that the isotherms were L- or H-type (Figure 7A-D).^{29,47} Both AN-BSA and AN-LSZ adsorption systems showed a L-type isotherm, while γ -PAN-BSA and γ -PAN-LSZ belonged to a H-type isotherm, which is an extreme case of L-type. Adsorption isotherms of L- or H-type commonly referred as Langmuir type isotherms indicated the adsorption of proteins onto AN or γ -PAN surface should involve chemical forces instead of physical interaction.²⁹ Following a rise in protein level from 500 to 5000 mg/L, the adsorption capacity climbed by 173.4 mg/g for AN-BSA, 11.2 mg/g for AN-LSZ, 30.7 mg/g for γ -PAN-BSA and 104 mg/g for γ -PAN-LSZ.

To gain more valuable information, the isotherms developed for all the four systems were fitted with the classical Langmuir isotherm model (Figure 7A-D) and the corresponding parameters were derived by a non-linear regression method (Table 1).^{28,29} The maximum adsorption capacity (q_{\max} , mg/g) was the highest for AN-BSA (224.5), followed by γ -PAN-LSZ (110.1), γ -PAN-BSA (36.1) and AN-LSZ (16.2). Apparently, the protein BSA was adsorbed more effectively onto AN surface, while LSZ adsorbed onto γ -PAN. However, the equilibrium constant (K_e , L/mg) followed the order: γ -PAN-LSZ (9.03×10^{-3}) > γ -PAN-BSA (8.58×10^{-3}) >

AN-BSA (1.38×10^{-3}) > AN-LSZ (0.60×10^{-3}), suggesting a drastic attainment of equilibrium for adsorption of BSA or LSZ onto γ -PAN. Nevertheless, a gradual rise in protein adsorption was shown for AN. The Langmuir constant K_e could be further incorporated into the equation for determination of the separation factor or dimensionless equilibrium parameter, $R_L = 1/(1 + K_e C_0)$ (Table 1).^{29,48} Also, the shape of isotherm could be evaluated based on 4 idealized equilibrium behaviors to be either unfavourable ($R_L > 1$) or linear ($R_L = 1$) or favorable ($0 < R_L < 1$) or irreversible ($R_L = 0$). The R_L values obtained were ranged from 0.127–0.936 for AN-BSA, 0.252–0.971 for AN-LSZ, 0.023–0.700 for γ -PAN-BSA and 0.022–0.689 for γ -PAN-LSZ, implying that a favorable adsorption ($0 < R_L < 1$) of proteins by AN and γ -PAN did occur. This tendency can be explained based on zeta potential and pH_{zpc} values of both nanoparticles and proteins. The zeta potential of BSA and LSZ at pH 6.9 was reported to be -13.6 ± 1.6 mV and $+7.9 \pm 0.6$ mV, respectively, with their pH_{zpc} values being 4.7–5.1 and 11.¹⁶ This outcome suggested a net negative and positive charge on BSA and LSZ, respectively, at the solution pH 7 used in our study. Moreover, from Figure 6, it was shown that AN possessed a positive surface charge with a zeta potential of +19.4 mV at pH 7, leading to high adsorption capacity (224.5 mg/g) through electrostatic attraction between the protonated AlOH groups on AN and negative charge of BSA surface. However, a low adsorption of only 16.2 mg of LSZ per g of AN did occur, which may be accounted for by the electrostatic repulsive force between positively charged surfaces on both AN and LSZ. Similar results were reported by several authors demonstrating marginal or no adsorption for LSZ by unfunctionalized AN.^{3,15,16}

Surface functionalization of AN not only provide strategy to control protein adsorption and broaden their applications,^{15,16} but also facilitate adsorption of oppositely charged proteins by charged functional groups, while protein-particle adsorption can also occur through interaction of hydrophobic/hydrophilic groups with water molecules.³ As

mentioned before, the functionalization of AN with γ -PGA enables introduction of ionizable carboxyl groups onto the AN surface, thereby making the γ -PAN surface negative owing to shift in zeta potential from +19.4 to -40.7 mV at pH 7.0 (Figure 6). Accordingly, γ -PAN can interact with LSZ possessing net positive charge via electrostatic attraction yielding high adsorption capacity (110.1 mg/g) compared with BSA (36.1 mg/g). However, the electrostatic repulsive force between γ -PAN and BSA could reduce the adsorption capacity greatly. In a study dealing with protein-particle adsorption, Meder *et al.*³ demonstrated that the adsorption of BSA occurred primarily through AIOH groups, whereas the carboxyl groups were mainly responsible for LSZ adsorption. Likewise, BSA molecules were shown to adsorb preferentially on bare AN and AN-NH₂, while the positively charged LSZ and TRY were readily adsorbed onto AN-COOH, AN-SO₃H and AN-PO₃H₂.¹⁵ Though the electrostatic forces appeared to dominate during adsorption, several other factors such as surface area and hydrophilic/hydrophobic nature of nanoparticle surface may also contribute to protein adsorption.¹⁷

It is worth pointing out that BSA is a soft protein composed of 188 ionizable carboxyl groups and 198 ionizable amino groups, while LSZ is a hard protein containing 9 ionizable carboxyl groups and 18 ionizable amino groups.¹⁶ Accordingly, localized positively charged arginin and lysine groups in BSA and negatively charged glutamic and aspartic acid groups in LSZ can contribute to adsorption of the former on γ -PAN and the latter on AN surfaces.¹⁶ Nonetheless, the charge distribution and number of available ionizable groups may be slightly different when a change in protein conformation occurred in adsorbed state or in solution, as pointed out by Brandes *et al.*⁴⁹ Besides, for γ -PAN-BSA system, it is also possible that BSA may adsorb on certain portions of γ -PAN surface slightly coated or uncoated with γ -PGA. All in all, this phenomenon is crucial for elucidating the fundamental

nanoparticle-protein interactions and the design of functionalized materials with tailored surface characteristics is imperative for biomedical and biotechnological applications.

3.4. Cytotoxicity towards prostate cancer cell and ROS formation

Cytotoxicity of both AN and γ -PAN towards human prostate cancer cell PC-3 was investigated for nanoparticle concentrations ranging from 0.01–1 mg/mL by MTT assay (Figure 8A). No significant toxicity occurred upon incubation of AN or γ -PAN with PC-3 cells for 24 h (data not shown). However, after incubating for 48 h, the cell viability dropped slightly for nanoparticle dose from 0.01–0.03 mg/mL, with no significant difference between AN and γ -PAN. When the dose was raised to 0.06, 0.13, 0.25, 0.50 and 1.00 mg/mL, the cell viability declined in a dose dependent manner by 13.5, 18.1, 25.1, 30.5 and 34.7% for AN, respectively, and 19.3, 27.3, 34.2, 40.3 and 47.7% for γ -PAN (Figure 8A). Obviously γ -PAN inhibited PC-3 proliferation more effectively than AN, which may be due to a better colloidal stability of the former.

Many reports dealing with metal oxide nanoparticles (ZnO, CuO, TiO₂, Fe₂O₃ and CeO₂) have been published, but to date only a few studies dealing with toxic effects of AN were carried out.^{20,50} From the toxicological point of view, the AN possessed minor toxicity towards plants, average toxicity for *Escherichia coli* and high toxicity against murine macrophage, while no toxicity was reported for selected mammalian cells (L929 and BJ) and rat alveolar macrophage (NR8383).²² Simon-Deckers *et al.*⁵¹ observed a low cytotoxicity of AN towards lung cancer cell A549, which was probably caused by rapid entry and distribution of AN into the cytoplasm and intracellular vesicles. Likewise, the AN size at 13 and 22 nm were shown to inhibit A549 cells through depolarization of cell membrane and the cell viability declined by 14.0 and 18.6% at 0.01 and 0.025 mg/mL, respectively, but without significant difference between two particle sizes.⁵ The cell viability data in our study revealed poor inhibition of PC-3 cells by AN or γ -PAN at low doses (0.01–0.03 mg/mL), however,

upon raising the nanoparticle dose over 0.06 mg/mL, the growth of PC-3 cells could be inhibited to a higher degree.

Many studies have demonstrated the induction of intracellular oxidative stress through production of various reactive oxygen species to be the key event involved in toxicity of many nanomaterials.^{20,50} The major constituents of ROS include superoxide anion radicals ($O_2^{\bullet-}$), hydroxyl radicals ($\bullet OH$) and hydrogen peroxide (H_2O_2).²⁰ Generally, ROS is produced as a byproduct of normal cell metabolism. However, under the severe stress conditions, the excessive production of ROS can lead to cell apoptosis or necrosis.⁵⁰ Nano-sized alumina particles have been shown to generate ROS to a greater extent than micro-sized particles resulting in more pro-inflammatory reactions and higher oxidative stress via intracellular signalling pathways.²⁰ Therefore, to measure ROS production upon exposure of AN and γ -PAN to PC-3 cells, nanoparticles with the same dose as cytotoxic study (0.01–1.00 mg/mL) were chosen (Figure 8B). There was no significant difference in ROS production during 24-h incubation, which is consistent with the cytotoxicity results. However, after 48 h incubation, an increase in ROS production following a rise in nanoparticle dose was observed. More specifically, when compared to the control treatment, the generation of ROS climbed from 583.6 to 1601.6% for AN and 806.3 to 1760.2% for γ -PAN, implying the latter could induce more ROS production than the former. The percentage difference in ROS production between AN and γ -PAN was 222.7, 322.7, 228.9, 139.9, 70.0, 126.5, 189.0 and 158.6 for doses at 0.01, 0.02, 0.03, 0.06, 0.13, 0.25, 0.5 and 1.0 mg/mL, respectively (Figure 8B). Taken together, the cytotoxicity of AN and γ -PAN towards PC-3 cells may be caused by generation of ROS leading to elevated oxidative stress. However, the percentage cytotoxicity towards PC-3 cells was not proportional to ROS generated at each nanoparticle dose, probably caused by difference in apoptotic signal transduction pathway. Theoretically the apoptosis of cancer cell caused by ROS production should be closely associated with mitochondria-mediated or

stress-mediated pathway. However, in our experiment it was suggested that the cytotoxicity towards PC-3 cells may also involve the death receptor-mediated pathway (extrinsic apoptosis pathway). In a recent review dealing with oxidative stress mediated toxicity, it was summarized that the toxicity of metal nanoparticles (Cu, Fe, Ag and Au) and metal oxide nanoparticles (CuO, Fe₂O₃, ZnO and TiO₂) was mediated by oxidative stress.²⁰ In other words, when the oxidative stress outweighs defense mechanisms, several cellular macromolecules such as proteins, lipids and DNA are subjected to destruction. It was also reported that metal oxide nanoparticles could perturb intracellular calcium homeostasis and activate macrophage inflammatory proteins and pro-inflammatory genes.⁵⁰ In addition, the cytotoxicity mechanism of AN towards A549 cells as studied by Lin *et al.*⁵ further demonstrated that the depolarization of cell membrane potential caused by ROS generation is mainly responsible for induction of oxidative stress. Likewise, in another study Chen *et al.*²³ reported that the cellular oxidative stress induced by loss of mitochondrial potential in human brain microvascular endothelial cells could disrupt the expression of tight junction proteins, while the primary DNA damage caused by pro-inflammatory effects induced by ROS was claimed to be responsible for cytotoxicity in two mammalian cells (L5178Y and BEAS-2B).²⁵ In addition to ROS determination, the changes in morphology of PC-3 cells upon treatment with different doses (0.01, 0.03, 0.13, 0.25, 0.50 and 1.00 mg/mL) of AN or γ -PAN alone (Figure 9A1-A13) and along with ROS detecting reagent CM-H₂DCFDA (Figure 9B1-B13) were monitored by capturing phase contrast images using inverted microscope. Visualization of images revealed no significant change in PC-3 cell morphology for all the above treatments, which is consistent with several reported studies demonstrating a negative influence on cell morphology upon treatment of cells with AN.⁵²⁻⁵⁵ Nevertheless, in these studies AN was shown to induce oxidative stress leading to apoptosis, DNA damage and protein degradation in vitro as well as alter neurobehavioral patterns in vivo.⁵²⁻⁵⁵ Thus, the

cytotoxicity of AN and γ -PAN towards PC-3 cells observed in this study should be closely associated with ROS generation, elevated oxidative stress and mitochondrial dysfunction. Nevertheless, more detailed study is required to elucidate the molecular mechanism involved in cytotoxicity of AN and γ -PAN.

4. Conclusions

Bare alumina nanoparticles (AN) and poly(γ -glutamic acid)-based alumina nanoparticles (γ -PAN) with a particle size of 6.7 nm was successfully prepared and evaluated for protein separation efficiency and toxicity towards human prostate cancer cell (PC-3). Among two model proteins tested for protein adsorption, AN preferentially adsorbed negatively-charged bovine serum albumin, while γ -PAN efficiently adsorbed positively-charged lysozyme. A relatively high adsorption of lysozyme on γ -PAN can facilitate the application of lysozyme-adsorbed γ -PAN as a promising antibacterial agent. A dose-dependent cytotoxicity towards human prostate cancer cell (PC-3) occurred for both nanoparticles through oxidative stress as evident by a concomitant rise in ROS level. This study could provide a basis for further screening of γ -PAN as a potential candidate for future biomedical applications.

Acknowledgements

The authors wish to thank Mr. Yen-Sheng Wu in Tzong Jao Hang's Electron Microscope Laboratory, School of Medicine, Fu Jen Catholic University, Taipei, Taiwan for technical assistance in recording transmission electron microscopic images.

References

- 1 G. Y. Tonga, K. Saha, V. M. Rotello, *Adv. Mater.* 2014, **26**, 359-370.
- 2 B. Pelaz, G. Charron, C. Pfeiffer, Y. Zhao, J. M. de la Fuente, X. J. Liang, W. J. Parak, P. Del Pino, *Small* 2013, **9**, 1573-1584.
- 3 F. Meder, S. Kaur, L. Treccani, K. Rezwan, *Langmuir* 2013, **29**, 12502-12510.

- 4 X. Ke, Y. Huang, T. R. Dargaville, Y. Fan, Z. Cui, H. Zhu, *Sep. Purif. Technol.* 2013, **120**, 239-244.
- 5 W. Lin, I. Staytona, Y. W. Huang, X. D. Zhoucand, Y. Maa, *Toxicol. Environ. Chem.* 2008, **90**, 983-996.
- 6 V. Piriyaawang, V. Thongpool, P. Asanithi, P. Limsuwan, *J. Nanomat.* 2012, Article ID 819403.
- 7 M. R. Karim, M. A. Rahman, M. A. J. Miah, H. Ahmad, M. Yanagisawa, M. Ito, *Open Coll. Sci. J.* 2011, **4**, 32-36.
- 8 H. Li, Y. Li, J. Jiao, H. M. Hu, *Nat. Nano* 2011, **6**, 645-650.
- 9 O. Saber, *Particuology* 2012, **6**, 744-750.
- 10 M. Khajeh, S. Laurent, D. Dastafkan, *Chem. Rev.* 2013, **113**, 7728-7768.
- 11 Rajaeiyan, M. B. Mohagheghi, *Adv. Manuf.* 2013, **1**, 176-182.
- 12 K. M. Parida, A. C. Pradhan, J. Das, N. Sahu, *Mater. Chem. Phys.* 2009, **113**, 244-248.
- 13 E. Casals, T. Pfaller, A. Duschl, G. J. Oostingh, V. Puentes, *ACS Nano* 2010, **4**, 3623-3632.
- 14 K. Rezwani, L. P. Meier, L. J. Gauckler, *Langmuir* 2005, **21**, 3493-3497.
- 15 F. Meder, T. Daberkow, L. Treccani, M. Wilhelm, M. Schowalter, A. Rosenauer, L. Maedler, K. Rezwani, *Acta Biomater.* 2012, **8**, 1221-1229.
- 16 F. Meder, C. Brandes, L. Treccani, K. Rezwani, *Acta Biomater.* 2013, **9**, 5780-5787.
- 17 L. Song, K. Yang, W. Jiang, P. Du, P. Xing, *Colloids Surf. B* 2012, **94**, 341-346.
- 18 F. Meder, H. Hintz, Y. Koehler, M. M. Schmidt, L. Treccani, R. Dringen, K. Rezwani, J. Am. Chem. Soc. 2013, **135**, 6307-6316.
- 19 X. B. Ke, R. F. Shao, H. Y. Zhu, Y. Yuan, D. J. Yang, K. R. Ratinacc, X. P. Gao, *Chem. Commun.* 2009, 1264-1266.
- 20 Sarkar, M. Ghosh, P. C. Sil, *J. Nanosci. Nanotechnol.* 2014, **14**, 730-743.
- 21 Y. J. Kim, H. S. Choi, M. K. Song, D. Y. Youk, J. H. Kim, J. C. Ryu, *Mol. Cell Toxicol.* 2009, **5**, 172-178.
- 22 E. Radziun, J. D. Wilczynska, I. Ksiazek, K. Nowak, E. L. Anuszevska, A. Kunicki, A. Olszyna, T. Zabkowski, *Toxicol. In Vitro* 2011, **25**, 1694-1700.

- 23 L. Chen, A. Robert, Yokel, B. Hennig, M. Toborek, *J. Neuroimmune Pharmacol.* 2008, **3**, 286-295.
- 24 S. T. Yang, T. Wang, E. Dong, X. X. Chen, K. Xiang, J. H. Liu, Y. Liu, H. Wang, *Toxicol. Res.* 2012, **1**, 69.
- 25 S. T. Kim, K. Saha, C. Kim, V. M. Rotello, *Acc. Chem. Res.* 2013, **46**, 681-691.
- 26 S. Bertazzo, W. F. Zambuzzi, H. A. da Silva, C. V. Ferreira, C.A. Bertran, *Clin. Oral Implan. Res.* 2009, **20**, 288-293.
- 27 S. Ghosh, H. Mashayekhi, B. Pan, P. Bhowmik, B. Xing, *Langmuir* 2008, **24**, 12385-12391.
- 28 B. S. Inbaraj, B. H. Chen, *Int. J. Nanomed.* 2012, **7**, 4419-4432.
- 29 Y. C. Rajan, B. S. Inbaraj, B. H. Chen, *J. Agric. Food Chem.* 2014, **62**, 4803-4811.
- 30 B. S. Inbaraj, J. S. Wang, J. F. Lu, F. Y. Siao, B. H. Chen. *Bioresour. Technol.* 2009, **100**, 200-207.
- 31 M. Stevanović, I. Savanović, V. Uskoković, S. D. Škapin, I. Bračko, U. Jovanović, D. Uskoković, *J. Colloid Interf. Sci.* 2014, **413**, 54-64.
- 32 H. M. Kim, H. Lee, K. S. Hong, M. Y. Cho, M. H. Sung, H. Poo, Y. T. Lin, *ACS Nano* 2011, **5**, 8230-8240.
- 33 B. S. Inbaraj, T. H. Kao, T. Y. Tsai, C. P. Chiu, R. Kumar, B. H. Chen, *Nanotechnol.* 2011, **22**, 0751011.
- 34 B. S. Inbaraj, B. H. Chen, *Bioresour. Technol.* 2011, **102**, 8868-8876.
- 35 K. S. Babu, M. Anandkumar, T. Y. Tsai, T. H. Kao, B. S. Inbaraj, B. H. Chen, *Int. J. Nanomed.* 2014, **9**, 5515-5531.
- 36 H. S. Potdar, K. W. Jun, J. W. Bae, S. M. Kim, Y. J. Lee, *Appl. Catal. A* 2007, **321**, 109-116.
- 37 R. Pournajaf, S. A. Hassanzadeh-Tabrizi, M. Ghashang, *Ceramics Int.* 2014, **40**, 4933-4937.
- 38 N. P. Sasidharan, P. Chandran, S. S. Khan, *Colloids Surf. B* 2013, **102**, 195-201.
- 39 Statistical Analysis System (SAS). SAS Procedures and SAS/Graph User's Guide, version 6, SAS Institute, Inc., Cary, NC, USA; 2011.
- 40 M. K. Naskar, *J. Am. Ceram. Soc.* 2010, **93**, 1260-1263.

- 41 O. Rahmanpour, A. Shariati, M. R. Nikou, *Int. J. Chem. Eng. Appl.* 2012, **3**, 125-128.
- 42 I. M. Sadiq, B. Chowdhury, N. Chandarsekaran, A. Mukherjee, *Nanomedicine: NBM* 2009, **5**, 282-286.
- 43 S. R. Ghanta, K. Muralidharan, *J. Nanopart. Res.* 2013, **15**, 1715.
- 44 R. Kumar, B. S. Inbaraj, B. H. Chen, *Mater. Res. Bull.* 2010, **45**, 1603-1607.
- 45 E. Illes, E. Tombacz, *J. Colloid Interf. Sci.* 2006, **295**, 115-123.
- 46 A. Shemetov, I. Nabiev, A. Sukhanova, *ACS Nano* 2012, **6**, 4585-4602.
- 47 G. H. Giles, T. H. MacEwan, S. N. Nakhwa, D. Smith, *J. Chem. Soc.* 1960, **111**, 3973-3993.
- 48 K. R. Hall, L. C. Eagleton, A. Acrivos, T. Vermeulen, *Ind. Eng. Chem. Fundam.* 1966, **5**, 212-219.
- 49 N. Brandes, P. B. Welzel, C. Werner, L. W. Kroh, *J. Colloid Interf. Sci.* 2006, **299**, 56-69.
- 50 Y. W. Huang, Ch. Wu, R. S. Aronstam, *Materials* 2010, **3**, 4842-4859.
- 51 Simon-Deckers, B. Gouget, M. Mayne-L'Hermite, N. Herlin-Boime, C. Reynaud, M. Carriere, *Toxicology* 2008, **253**, 137-146.
- 52 M. C. Hofmann, in *Nanomaterial: Impacts on Cell Biology and Medicine*, ed. D. G. Capco and Y. S. Chen, Springer, New York, 2014, ch. 13, pp. 255-275.
- 53 S. J. Choi, J. M. Oh, J. H. Choy, *J. Inorg. Biochem.* 2009, **103**, 463-471.
- 54 I. S. Kim, M. Baek, S. J. Choi, *J. Nanosci. Nanotechnol.* 2010, **10**, 3453-3458.
- 55 Q. L. Zhang, M. Q. Li, J. W. Ji, F. P. Gao, R. Bai, C. Y. Chen, Z. W. Wang, C. Zhang, Q. Niu, *Int. J. Immunopathol. Pharmacol.* 2011, **24**, 23S-29S.

FIGURE CAPTIONS

Figure 1 X-ray diffraction pattern for γ -alumina nanoparticles (A) and γ -PGA coated γ -alumina nanoparticles (B)

Figure 2 Transmission electron microscopic images of γ -alumina nanoparticles (A) and γ -PGA coated γ -alumina nanoparticles (B) recorded at 120 kV along with an inset showing particle-size distribution histogram directly obtained from the corresponding image.

Figure 3 Scanning electron microscopic images of γ -alumina nanoparticles (A1) and γ -PGA coated γ -alumina nanoparticles (B) along with electron dispersive X-ray spectra obtained in mapping mode to visualize proportion of aluminium (A2 and B2), carbon (A3 and B3) and oxygen (A4 and B4).

Figure 4 Fourier transform infrared spectra of boehmite (A), γ -alumina nanoparticles (B), pure γ -PGA (C) and γ -PGA coated γ -alumina nanoparticles (D).

Figure 5 Thermogravimetric analyses of γ -alumina and γ -PGA coated γ -alumina nanoparticles.

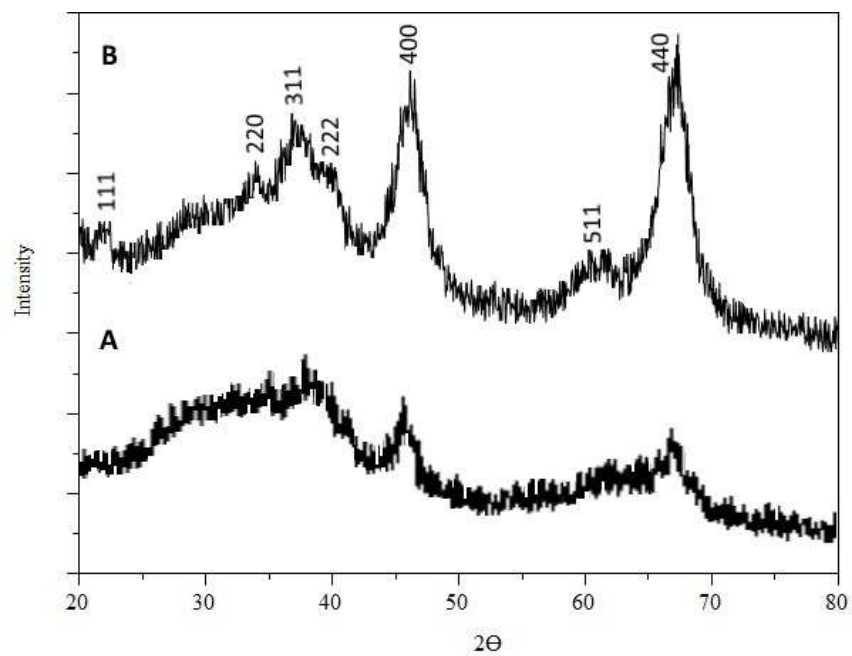
Figure 6 Zeta potential analyses of γ -alumina and γ -PGA coated γ -alumina nanoparticles as affected by different solution pH.

Figure 7 Protein adsorption isotherms for bovine serum albumin and lysozyme by γ -alumina nanoparticles (A and B) as well as γ -PGA coated γ -alumina nanoparticles (C and D).

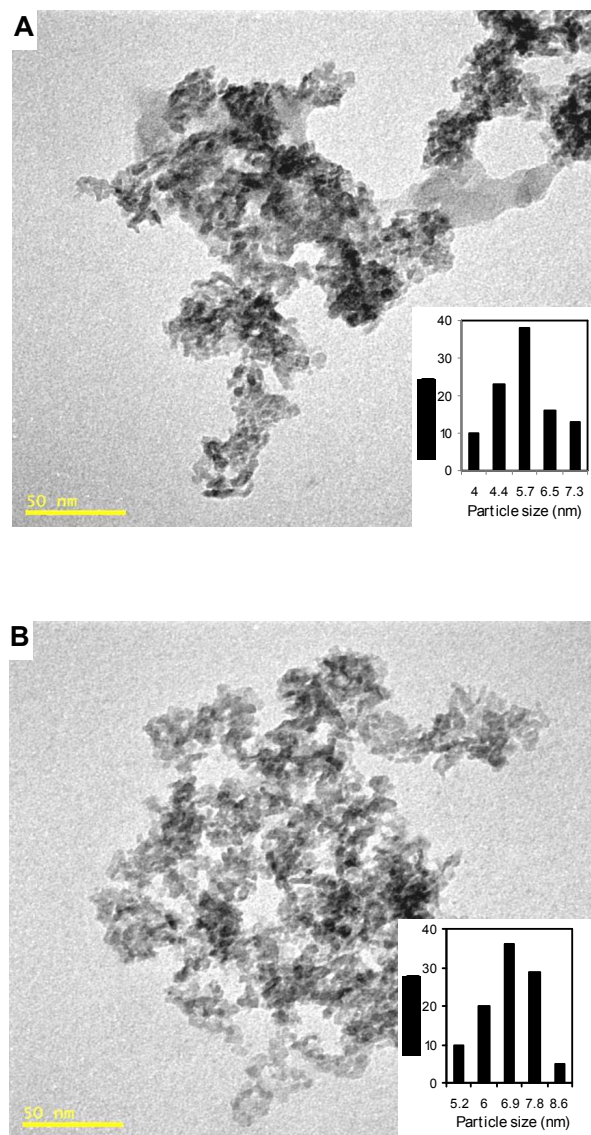
Figure 8 Cytotoxicity of γ -alumina and γ -PGA coated γ -alumina nanoparticles towards PC-3 human prostate cancer cell by MTT assay (A) and intracellular reactive oxygen species formation (B) after 48 h incubation.

Figure 9 Phase contrast images captured using inverted microscope during determination of intracellular reactive oxygen species. (A1) control PC-3 cells, (A2-A7) PC-3 cells treated with different concentrations of γ -alumina nanoparticles, (A8-A13) PC-3 cells treated with different concentrations of γ -PGA coated γ -alumina nanoparticles, (B1) Control PC-3 cells treated with ROS detecting reagent CM-H₂DCFDA only, (B2-B7) PC-3 cells treated with different concentrations of γ -alumina nanoparticles followed by CM-H₂DCFDA, (B8-B13) PC-3 cells treated with different concentrations of γ -PGA coated γ -alumina nanoparticles followed by CM-H₂DCFDA. The panels A2 and B2, A3 and B3, A4 and B4, A5 and B5, A6 and B6, and A7 and B7 denote different doses of γ -alumina nanoparticles at 0.01, 0.03, 0.13, 0.25, 0.50 and 1.00 mg/mL, respectively, while A8 and B8, A9 and B9, A10 and B10, A11

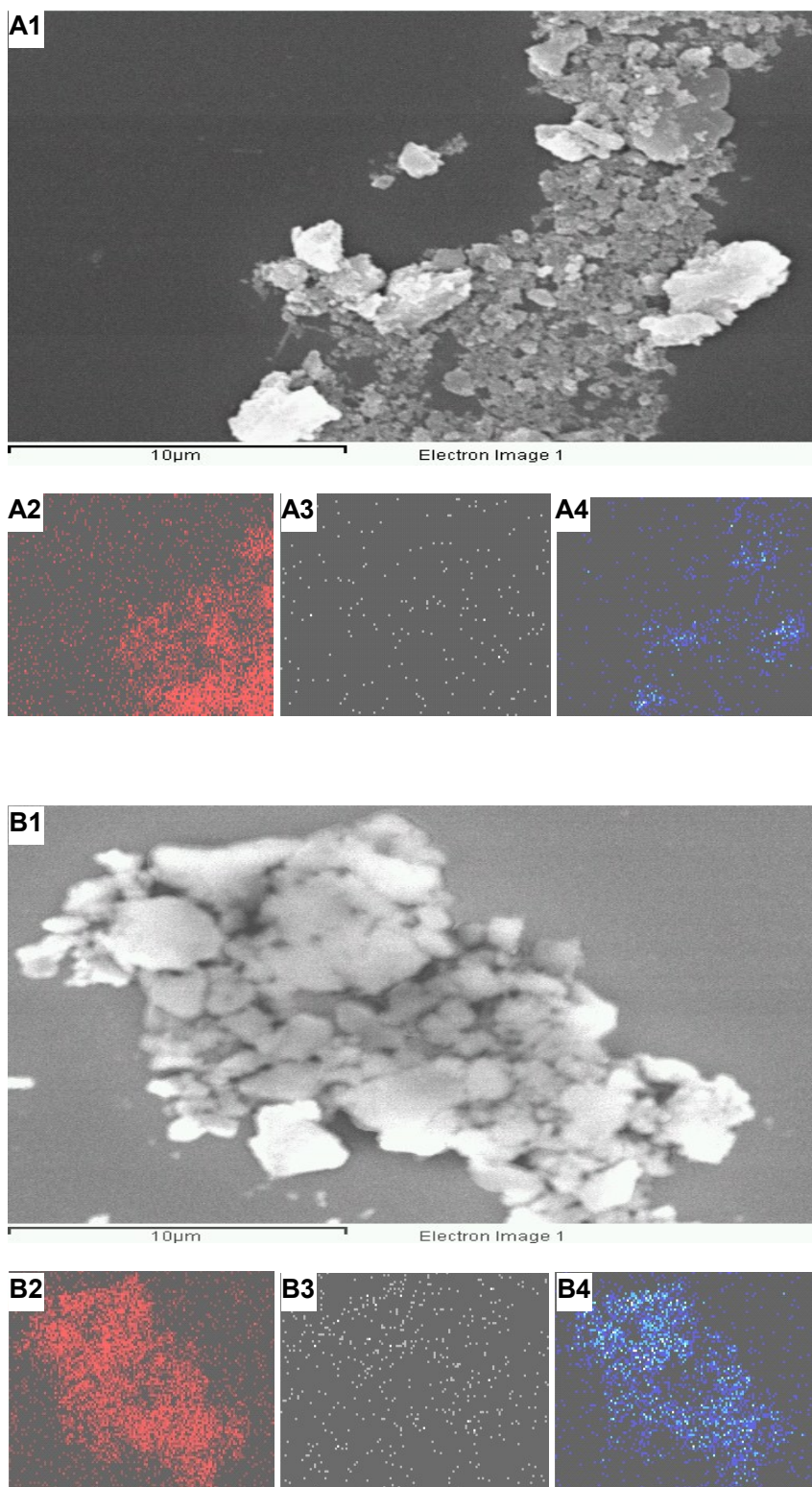
and B11, A12 and B12, and A13 and B13 represent the same corresponding doses of γ -PGA coated γ -alumina nanoparticles.



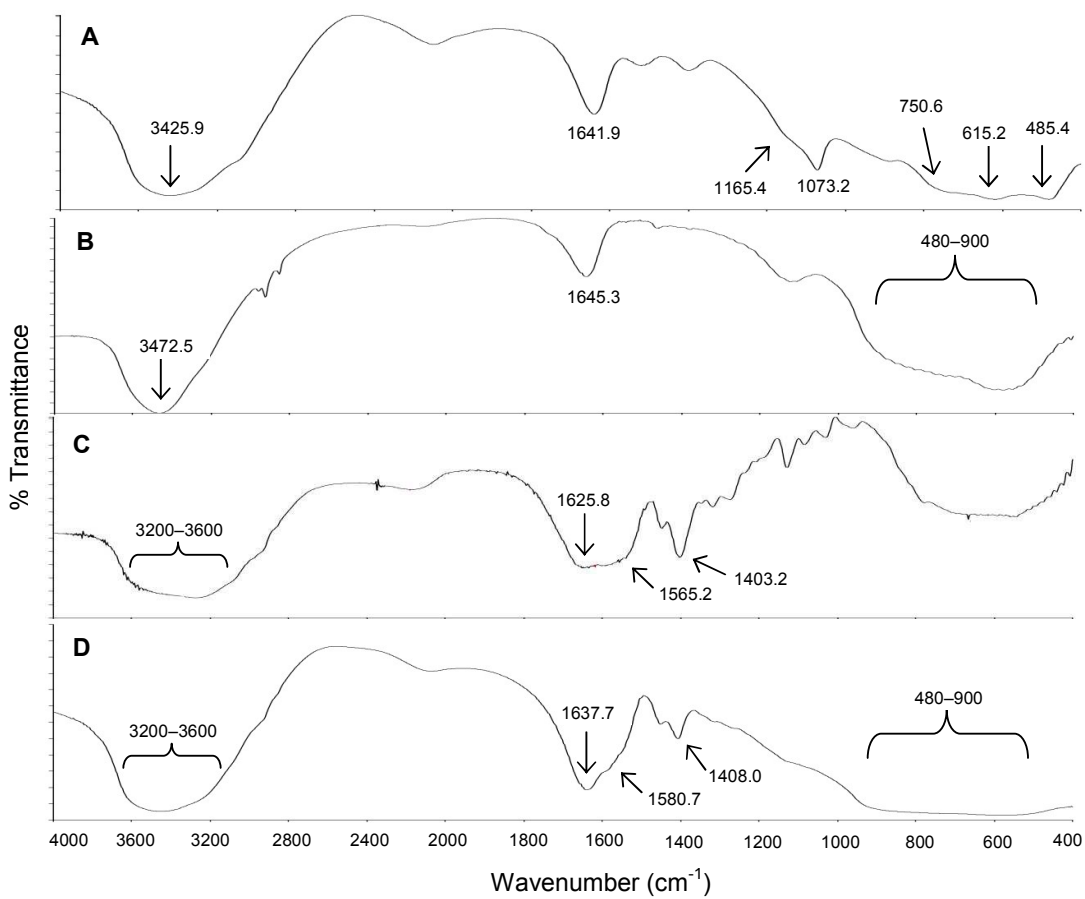
(FIGURE – 1)

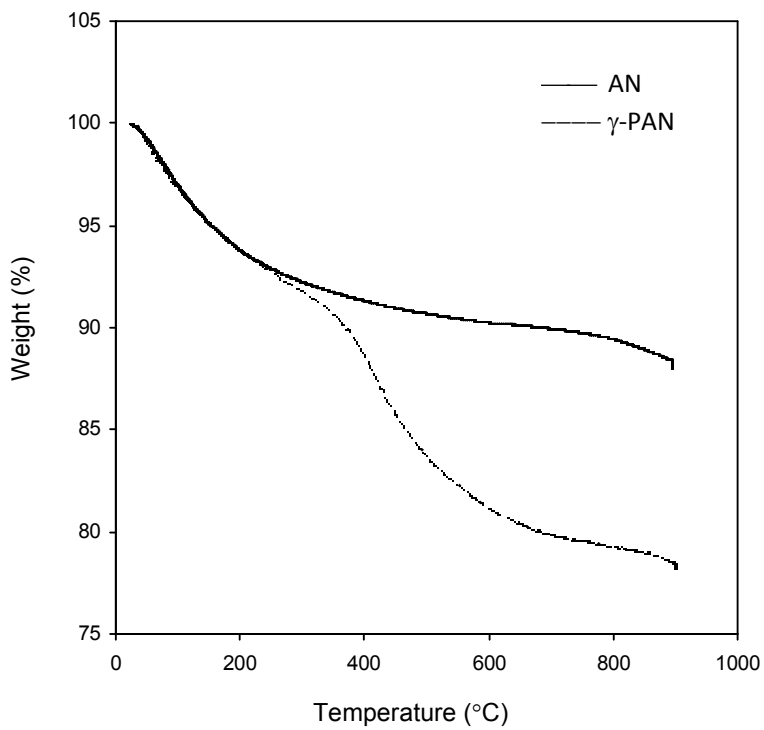


(FIGURE – 2)

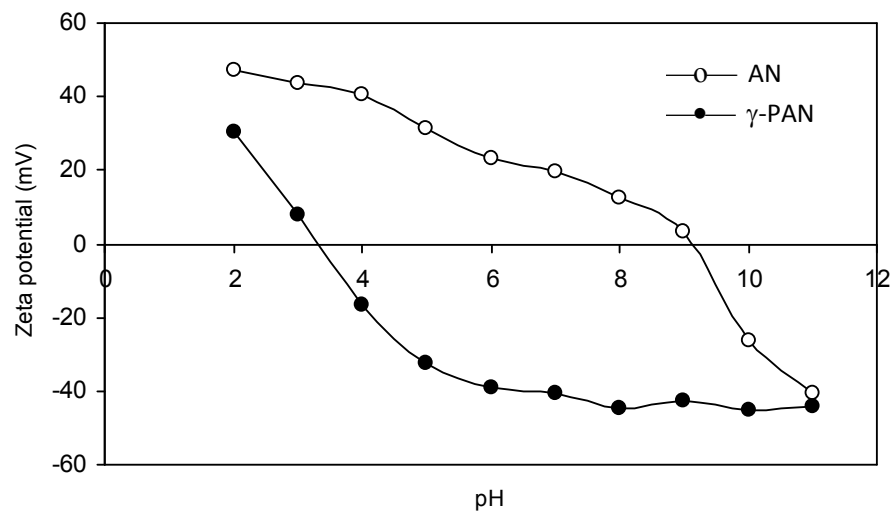


(FIGURE -3)

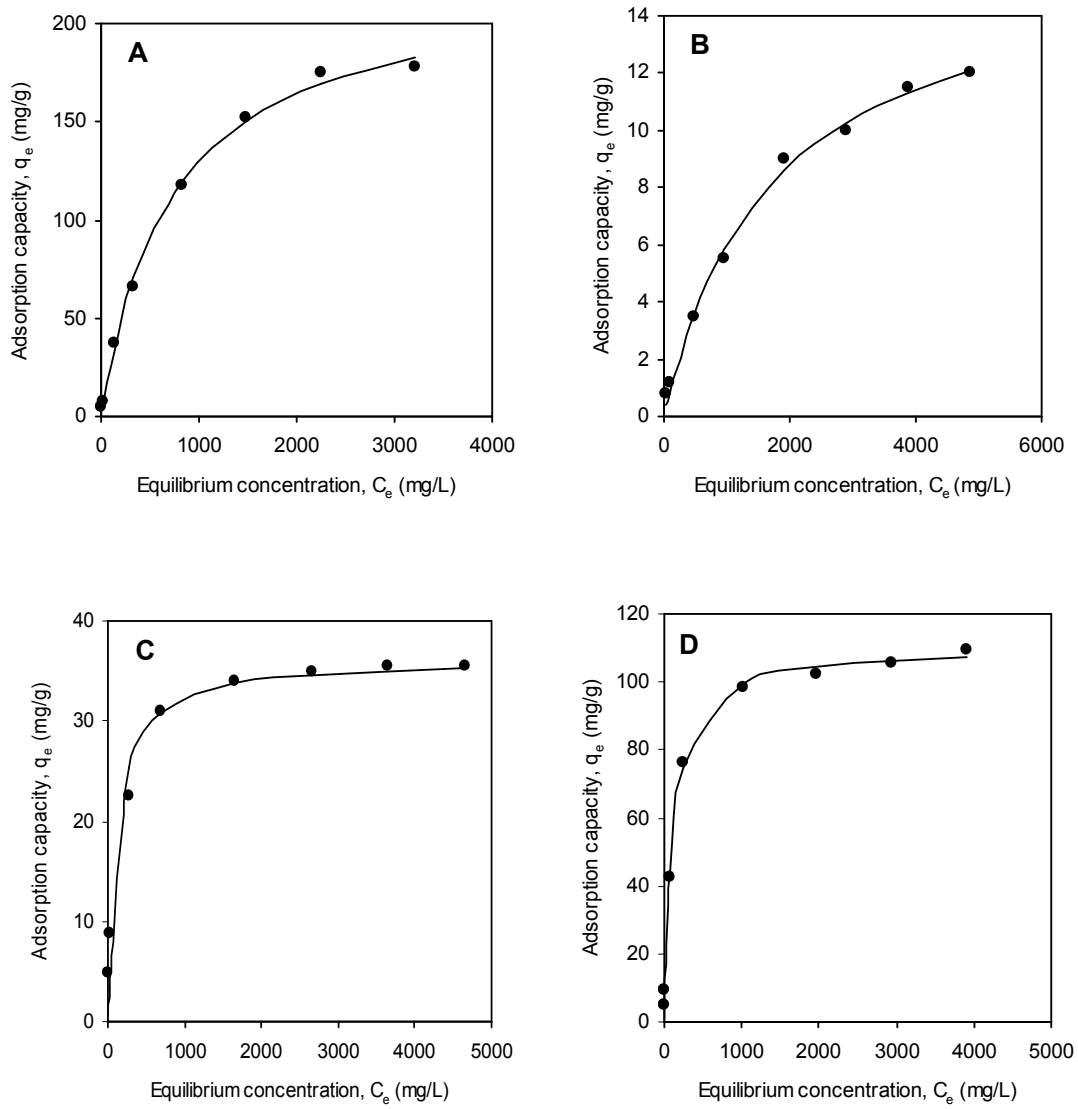
**(FIGURE - 4)**



(FIGURE - 5)



(FIGURE - 6)

**(FIGURE - 7)**

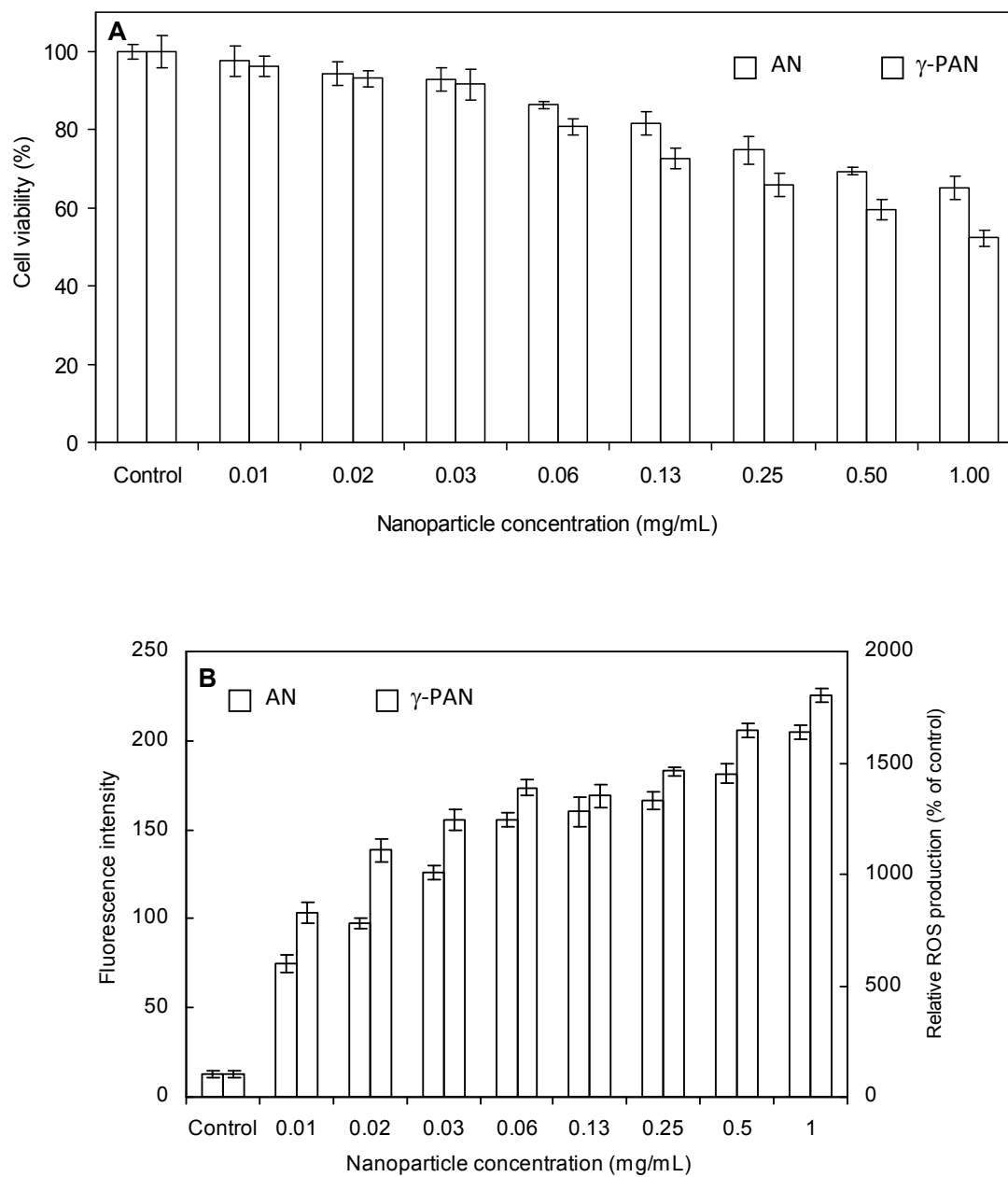


(FIGURE – 8)

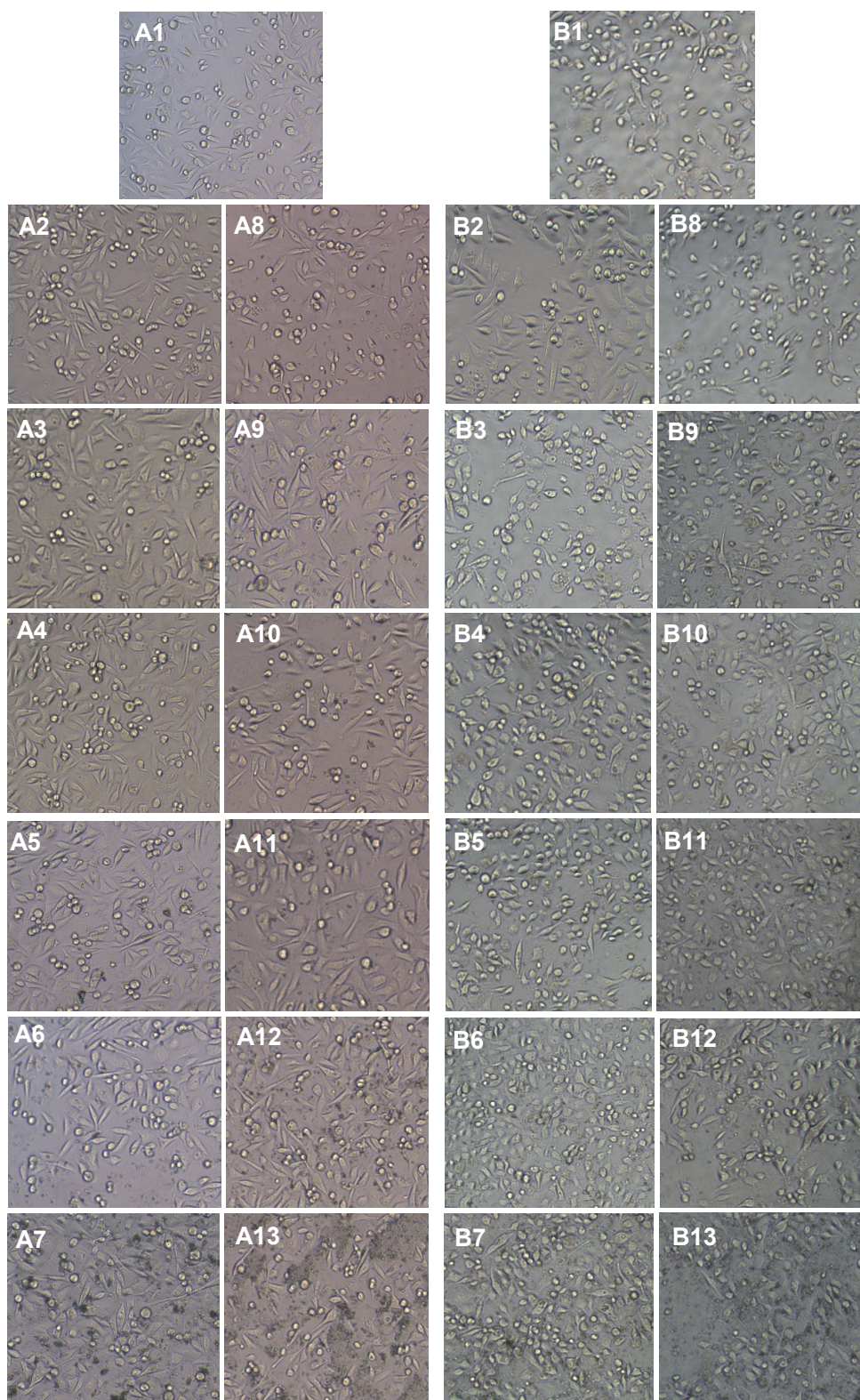
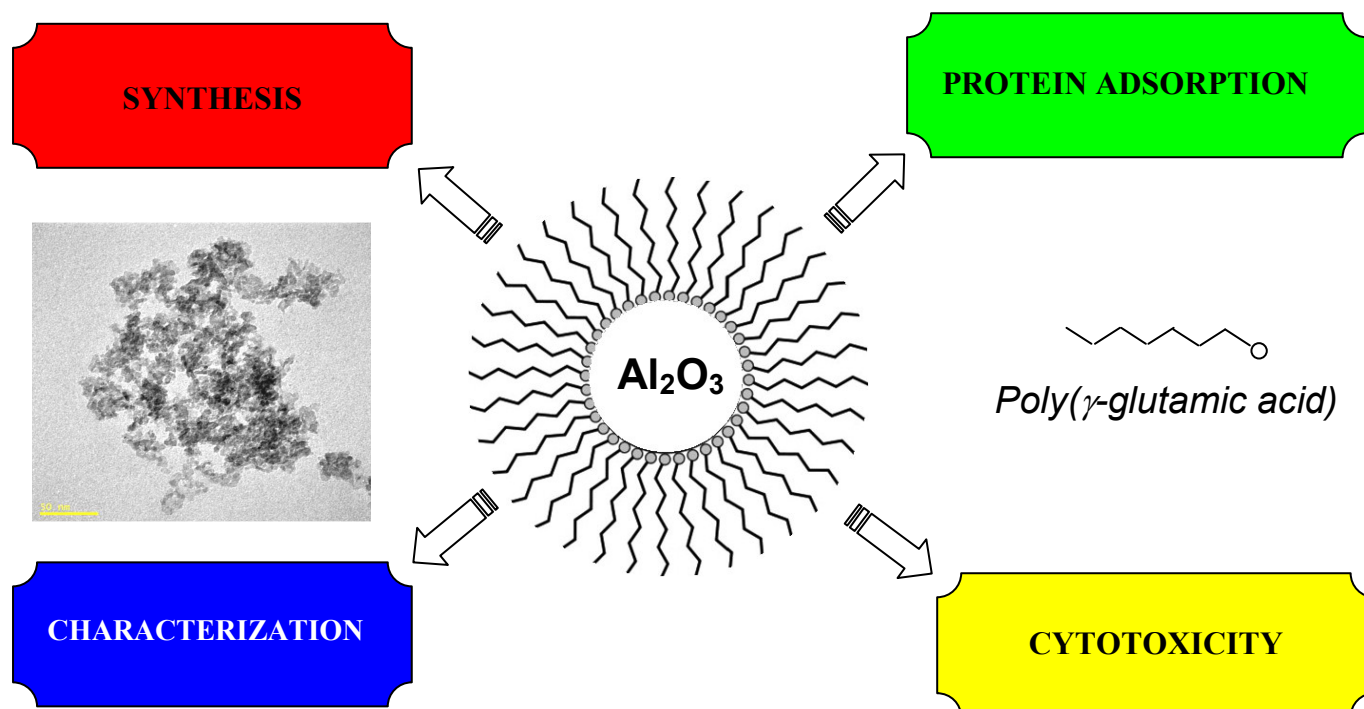


(FIGURE – 9)

Table 1. Non-linear regression parameters for the Langmuir isotherm modelling of protein adsorption by γ -alumina nanoparticles and γ -PGA coated γ -alumina nanoparticles

Nanoparticle	Protein	Modelled Langmuir isotherm parameters*				
		K_L (L/g)	q_{max} (mg/g)	K_e (L/mg)	r^2	R_L
γ -alumina	Bovine serum albumin	0.309	224.5	1.38×10^{-3}	0.997	0.127-0.936
	Lysozyme	0.010	16.2	0.60×10^{-3}	0.996	0.252-0.971
γ -PGA coated γ -alumina	Bovine serum albumin	0.310	36.1	8.58×10^{-3}	0.983	0.023-0.700
	Lysozyme	0.994	110.1	9.03×10^{-3}	0.998	0.022-0.689

* The non-linear isotherm model along with the definition of each modelled parameters are provided in the text.



Protein adsorption and cytotoxicity of poly(γ -glutamic acid) functionalized nanoalumina